# Supporting Information

# Development of Gold Phosphorus Supported Carbon Nanocomposites

**Vishal J. Mayani, Suranjana V. Mayani, and Sang Wook Kim***

*Department of Advanced Materials Chemistry, College of Science and Technology, Dongguk University-Gyeongju, Gyeongbuk 780-714, Korea. *E-mail: swkim@dongguk.ac.kr*
*Received September 24, 2013, Accepted November 7, 2013*

## 1. Synthesis of Carbon Gold Phosphorus Nanocomposite (CGPN) Materials:

Figure 1 represents the schematic diagram of preparation of two sized (25 and 170 nm) nano silica ball (NSB), carbon cage (CC), carbon silica nanocomposite (CSN), carbon gold nanocomposite (CGN), carbon phosphorus nanocomposite (CPN) and carbon gold phosphorus nanocomposite (CGPN) materials from low-cost pyrolysis fuel oil (PFO) based pitch.

**Preparation of Nano Silica Ball (NSB-25/170).** Nano silica ball (NSB) was prepared by hydrolysis and condensation of TEOS. Here, we have synthesized two sets of NSB (25 nm and 170 nm). In a typical synthesis of NSB-25, 10 mL distilled water and 7.8 mL of TEOS were stirred (400 rpm) in 500 mL of absolute ethanol (EtOH) for 30 min. 4 mL of $NH_4OH$ (28 wt %) was added to the resulting mixture, which was left to stir for further 24 h at room temperature at 400 rpm. The reaction mixture was transferred to oven and heated at 70 °C until complete dryness. The solid product was washed (ethanol and warm water) and dried at room temperature in air. The resulted NSB-25 were calcined at 550 °C for 6 h. (NSB-25); yield (2.3 g), BET surface area of NSB-25: 30 $m^2$/g, FTIR (KBr) 811, 1104, 1627, 1870, 3439, 3746 $cm^{-1}$. (NSB-170); yield (6.1 g), BET surface area of NSB-170: 163 $m^2$/g, FTIR (KBr) 469, 553, 799, 949, 1096, 1396, 1632, 3430 $cm^{-1}$.[1]

**Synthesis of Carbon Cage (CC-25/170).** The CC-25/170 materials were prepared as shown in Figure 1. The pitch residue, used as a CC precursor, was prepared according to the method reported previously under a heat extraction and self-crystallization method.[2] For a typical procedure, 12 g of pitch was heated at 50 °C and mixed homogeneously with 10 g of NSB-25/NSB-170 in crucible for 10 min. After cooling to room temperature, the mixture was carbonized at 900 °C for 4 h under nitrogen atmosphere to produce the carbon silica nanocomposite (**CSN-25/170**) material. The resulting CSN-25/170 material was treated with 10% hydrofluoric acid (HF) for 12 h. The solid carbon cage (CC-25/170) material was washed with distilled water and followed by drying at 100 °C in oven. (CC-25); yield (6.3 g), BET surface area of CC-25: 82 $m^2$/g, FTIR (KBr) 1113, 1584, 1620, 3437 $cm^{-1}$. Elemental analysis results showed that CC-25 contained > 94 wt % carbon and < 1.2 wt % H after carbonization at > 900 °C. (CC-170); yield (6.2 g), BET surface area of CC-170: 212 $m^2$/g, FTIR (KBr) 811, 1099, 1257, 1602, 3453 $cm^{-1}$. Elemental analysis results showed that CC-170 contained > 95 wt % carbon and < 0.4 wt % H after carbonization at > 900 °C.[3]

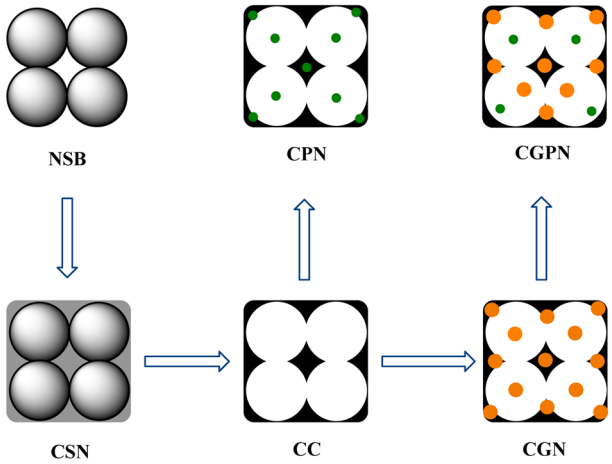


**Figure 1.** Schematic illustration for the synthesis of NSB, CC, CGN, CPN and CGPN.

**Synthesis of Carbon Gold Nanocomposite (CGN-25/170).** In order to prepare the **CGN-25/170,** 3.07 g of CC-25/170 were added in 250 mL of sodium citrate dihydrate solution and the mixture was then exposed to ultrasonic process for 5 min. The suspension of CC-25/170 was then transferred to 250 mL of distilled water. The diluted suspension was refluxed with stirring for 5 min, followed by the addition of 1% $HAuCl_4$ (100 mL) to the suspension containing CC-25/170. The resulting suspension was stirred at boiling temperature for next 5 min. The resulting solid particles were filtered with a Buchner funnel and washed with distilled water. The powder was dried in air at 100 °C. Finally, the solid was calcined at 900 °C for 1 h in nitrogen to yield **CGN-25/170** (Figure 1). (CGN-25); Yield: 3.5 g, BET surface area of CGN-25: 75 $m^2$/g, FTIR (KBr) 1119, 1254, 1579, 3449 $cm^{-1}$. Elemental analysis and ICP results showed that CGN-25 contained > 85 wt % carbon and > 11.0. wt % Au after carbonization at > 900 °C. (CGN-170); Yield: 3.6 g, BET surface area of CGN-170: 184 $m^2$/g, FTIR (KBr) 806, 1116, 1590, 3487 $cm^{-1}$. Elemental analysis and ICP results showed that CGN-170 contained > 86 wt % carbon and > 10.2 wt % Au after carbonization at > 900 °C.[3]

**Synthesis of Carbon Phosphorus Nanocomposite (CPN-25/170).** Typically, 3 g of CC-25/170 was mixed with 10 mL

of distilled water in a beaker followed by addition of 0.4 mL of $H_3PO_4$ solution (85%). The resulting suspension was exposed to ultrasonication for 10 min. The process was followed by evaporation of excess water and drying in oven at 140 °C for 12 h. The material was activated at 800 °C for 30 min in tubular furnace in presence of argon gas. After activation, the phosphorus-impregnated carbon nano composite was cooled to room temperature in a flow of argon. To remove the excess $H_3PO_4$, the samples were extensively washed with hot water in Soxhlet extractor until the pH of the washing become neutral. Then sample were dried in oven at 110 °C. Finally, it gave a black color carbon phosphorus nanocomposite (**CPN-25/170**) with high carbon content. (CPN-25); Yield: 3.3 g, BET surface area of CPN-25: 70 $m^2$/g, FTIR (KBr) 1084, 1206, 1580, 3434 $cm^{-1}$. Elemental analysis and ICP results showed that CPN-25 contained > 72 wt % carbon and > 0.9 wt % phosphorus (P) after activation at 800 °C. (CPN-170); Yield: 3.4 g, BET surface area of CPN-170: 178 $m^2$/g, FTIR (KBr) 1229, 1586, 3498 $cm^{-1}$. Elemental analysis and ICP results showed that CPN-170 contained > 82 wt % carbon and >1.5 wt % phosphorus (P) after activation at 800 °C.

**Synthesis of Carbon Gold Phosphorus Nanocomposite (CGPN-25/170).** In the mixture of distilled water (10 mL) and 3 g of CGN-25/170, add 0.4 mL of $H_3PO_4$ solution (85%) and sonicate it for 10 min. The process was followed by evaporation of excess water and drying in oven at 140 °C for 12 h. The material was activated at 800 °C for 30 min in tubular furnace through argon gas purging. Later, the resultant nanocomposite was cooled to room temperature in a flow of argon. The excess reactant $H_3PO_4$ was removed by extensively water washing until neutral pH through Soxhlet extraction. The material was dried in oven at 110 °C to obtain carbon gold phosphorus nanocomposite **(CGPN-25/170)** material. (CGPN-25); Yield: 3.4 g, BET surface area of CGPN-25: 40 $m^2$/g, FTIR (KBr) 1084, 1216, 1579, 3427 $cm^{-1}$. Elemental analysis and ICP results showed that CGPN-25 contained > 71 wt % carbon with > 10.9 wt % gold (Au) and > 0.9 wt % phosphorus (P) after activation at 800 °C. (CGPN-170); Yield: 3.4 g, BET surface area of CGPN-170: 172 $m^2$/g, FTIR (KBr) 1183, 1580, 3486, 3678 $cm^{-1}$. Elemental analysis and ICP results showed that CGPN-170 contained > 75 wt % carbon with > 4.8 wt % gold (Au) and > 3.3 wt % phosphorus (P) after activation at 800 °C.

## Materials, Characterization and Analysis

Pyrolysis fuel oil (PFO) was obtained from YNCC (Yeocheon Naphtha Cracking Center, Korea). Other chemicals such as ethanol, toluene, ammonium hydroxide, phosphoric acid (85%), sodium citrate dehydrate, (Dae-Jung Chemicals & Metals Co. Ltd., Korea), tetraethylorthosilicate (TEOS) (Aldrich, USA), hydrofluoric acid (J. T. Baker, USA) and hydrogen tetrachloroaurate (III) hydrate ($HAuCl_4$) (Kojima Chemicals Co. Ltd, Japan) were used as received. All the solvents were purified by known method.[4]

The different sized (25 and 170 nm) materials NSB, CC, CGN, CPN and CGPN were characterized by powder X-ray diffraction (PXRD, Phillips X'pert MPD diffractometer, Almelo, The Netherlands) in 2θ range (1-10 and 10-80) at scan step 0.02°. Fourier transfer infrared spectra were completed (FT-IR, Perkin-Elmer FTIR Spectrometer, Massachusetts, USA) using KBr self supported pellet technique. Microanalysis of the products was carried out by a CHN analyzer (CE instruments, UK) and the metals entering into the carbon cage was determined with inductively coupled plasma-optical emission spectroscopy (ICP-OES, JY Ultima 2CHR). BET surface area was determined by $N_2$-sorption data measured at 77 K using volumetric adsorption set up (Micromeritics ASAP-2010, USA). The pore diameter of the samples was determined from the desorption branch of nitrogen adsorption isotherm employing the Barret-Joyner-Halenda (BJH) model. Thermal measurements and microstructure evaluation of these samples were carried out on thermo-gravimetric analyzer (TGA, SDT600, TA instrument, USA) and scanning electron microscopy coupled with energy dispersive spectroscopy (SEM-EDX, LEO-1430, VP, UK), transmission electron microscopy (TEM, JEM 2011, Jeol Corporation, Japan).

**Characterization by Powder X-ray Diffractions.** Low-angle and wide-angle powder X-ray diffractions (PXRD) were used to characterize the all nanocomposites. Low-angle PXRD (1-10°) measurement did not produce any characteristic peak which indicates short range order or disordered phases present in the all hybrid nanocomposites prepared (Figures 2 and 3).

The wide-angle PXRD profile of NSB-25 showed (Figure 4) one broad peak assigned at 2θ = 23.3°, corresponding to the diffraction peak of amorphous silica .5 Two additional peaks, with lower intensity corresponding to graphite-type reflection from the (002) and (100) planes, were observed at 2θ values of 24.9° and 42.9°, respectively, upon switching to CC-25 from NSB-25.[5,6] The XRD of the CGN-25 material showed four additional peaks at 2θ = 38.2°, 44.4, 64.6° and 77.6°, which corresponded to reflections of Au planes (111), (200), (220) and (311) respectively, denoting the formation of noble gold particles with a face centered cubic structure.[7,8] The XRD measurement of CPN-25 did not show any additional characteristic peak except graphite-type reflection from the (002) and (100) planes of CC-25. Similarly, CGPN-25 shown marginally shifted XRD peaks at 2θ = 25.3°, 39.2°, 45.6°, 66.3° and 79.9°, which corresponded to reflections of Au plans. All the nano composites exhibits broad peaks centered at 2è value of around 20-30° which is consistent with typical amorphous nature of the silica/carbon foundation. The XRD spectra recoded in the examined area of CGN-25 and CGPN-25 nanocomposites have shown strong signals for gold in carbon foundation.

The wide-angle PXRD profile of NSB-170 showed (Figure 5) one broad peak assigned at 2θ = 21.3°, corresponding to the diffraction peak of amorphous silica.[5] Two additional peaks, with lower intensity corresponding to graphite-type reflection from the (002) and (100) planes,

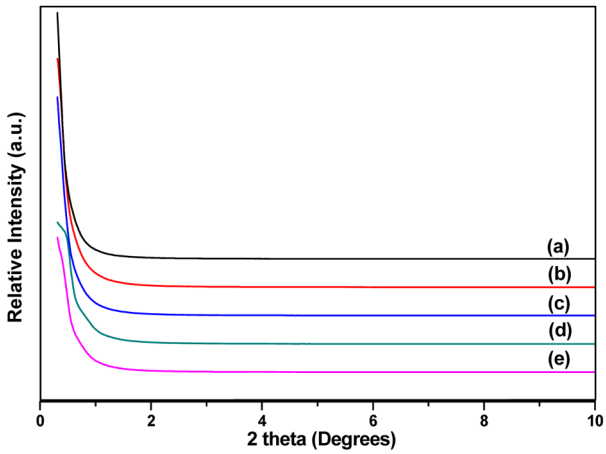


**Figure 2**. Low-angle PXRD patterns of NSB-25 (a), CC-25 (b), CGN-25 (c), CPN-25 (d) and CGPN-25 (e).

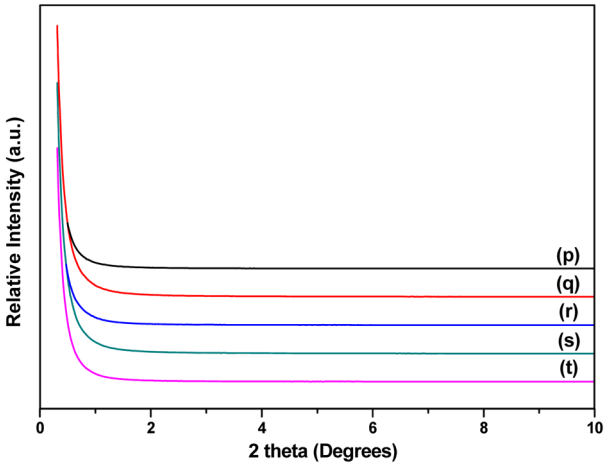


**Figure 3**. Low-angle PXRD patterns of NSB-170 (p), CC-170 (q), CGN-170 (r), CPN-170 (s) and CGPN-170 (t).

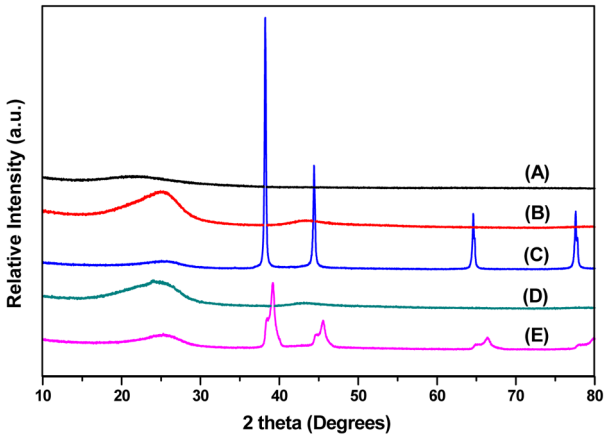


**Figure 4.** Wide-angle PXRD patterns of NSB-25 (A), CC-25 (B), CGN-25 (C), CPN-25 (D) and CGPN-25 (E).

were observed at 2θ values of 25.2° and 43.2°, respectively, upon switching to CC-170 from NSB-170.[5,6] The XRD of the CGN-170 material showed four additional peaks at 2θ = 38.2°, 44.4, 64.6° and 77.6°, which corresponded to reflections of Au planes (111), (200), (220) and (311)

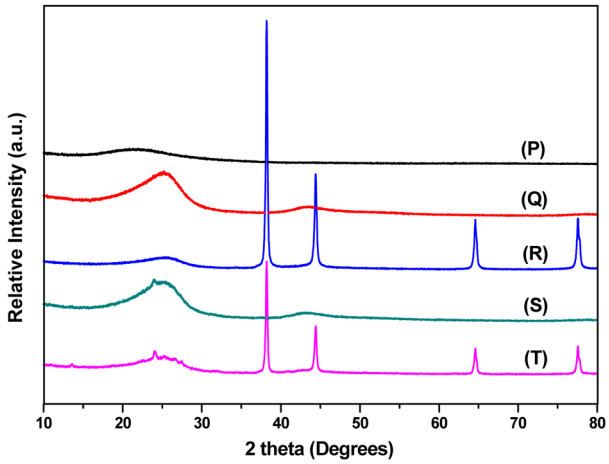


**Figure 5.** Wide-angle PXRD patterns of NSB-170 (P), CC-170 (Q), CGN-170 (R), CPN-170 (S) and CGPN-170 (T).

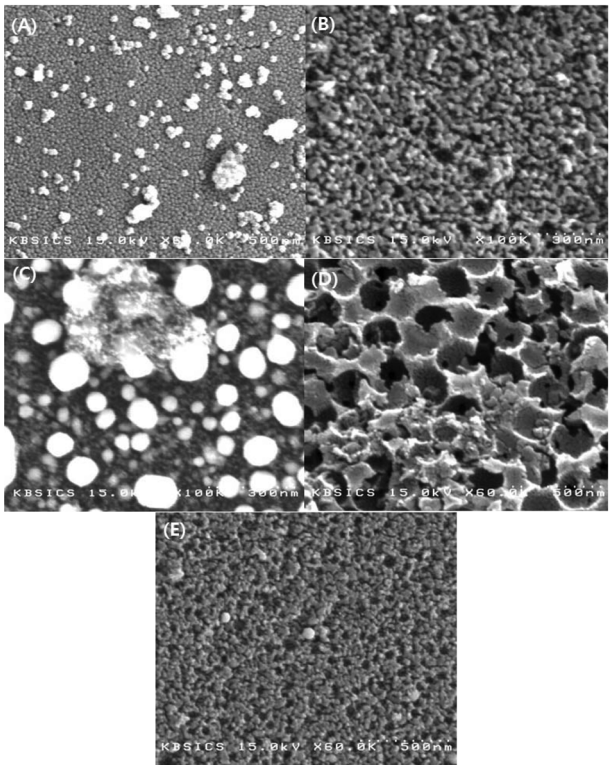


**Figure 6.** SEM images of NSB-25 (A), CC-25 (B), CGN-25 (C), CPN-25 (D) and CGPN-25 (E).

respectively, denoting the formation of noble gold particles with a face centered cubic structure.[7,8] The XRD spectra of CPN-170 measurement did not show any additional characteristic peak except graphite-type reflection from the (002) and (100) planes of CC-170 at 2θ values of 23.9° and 43.0°, respectively. Similarly, CGPN-25 shown XRD peaks at 2θ = 24.1°, 25.3°, 38.2°, 44.4°, 64.6° and 77.6°, which corresponded to reflections of Au plans. All the hybrid carbon nanocomposites revealed broad peaks centered at 2θ value of around 20-30° which is consistent with typical amorphous nature of the silica/carbon matrix.

**Characterization by SEM Analysis.** The structural

morphology of the NSB, CC, CGN, CPN and CGPN (25 nm and 170 nm) were investigated by SEM and TEM analysis. The SEM image of NSB-25 (Figure 6(A)) showed that most particles were uniform, spherical with particle size diameter ~25 nm and closely packed with each other. While SEM images of CC-25 revealed hollow cores of ~25 nm in diameter with interconnected hierarchically porous structure (Figure 6(B)).[9] They become more regular and smooth after thermal treatment. Additionally, CGN-25, CPN-25 and CGPN-25 showed well stabilized Au, P and combined (Au-P) particles on CC-25 with narrow particle diameter, respectively (Figures 6(C), 6(D) and 6(E)). Hybrid metal containing nanocomposites shown a clear difference between the carbon cage and the metal/non-metal elements (Au, P and Au-P) nano particles present on the CC-25 backbones. The hierarchically porous composite materials (CC-25) synthesized by the templating approach suggest that the spherical morphology is well-replicated.

The SEM image of NSB-170 (Figure 7(a)) showed that most particles were uniform, spherical with particle size diameter ~170 nm and closely packed with each other. While SEM images of CC-170 revealed hollow cores of ~170 nm in diameter with interconnected hierarchically porous structure (Figure 7(b)).[9] They become more regular and smooth after thermal treatment. Additionally, CGN-170, CPN-170 and CGPN-170 exhibited well-stabilized Au, P and combined (Au-P) particles on CC-170 with little wider particle diameter, respectively. All hybrid metal supported nanocomposites shown a clear difference between the carbon cage and the metal/non-metal (Au, P and Au-P) nano particles present on the CC-170 backbones along with replicated hollow and spherical morphology of NSB-170 (Figures 7(c), 7(d) and 7(e)).

The SEM was coupled with energy dispersive spectroscopy (EDS) to assess the purity and the elemental composition of composite materials (Figure 8). The EDS

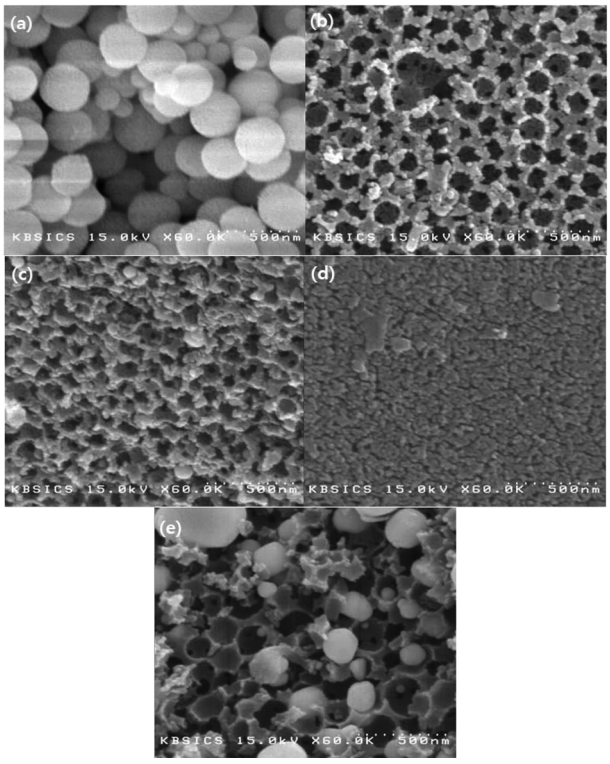


**Figure 7.** SEM images of NSB-170 (a), CC-170 (b), CGN-170 (c), CPN-170 (d) and CGPN-170 (e).

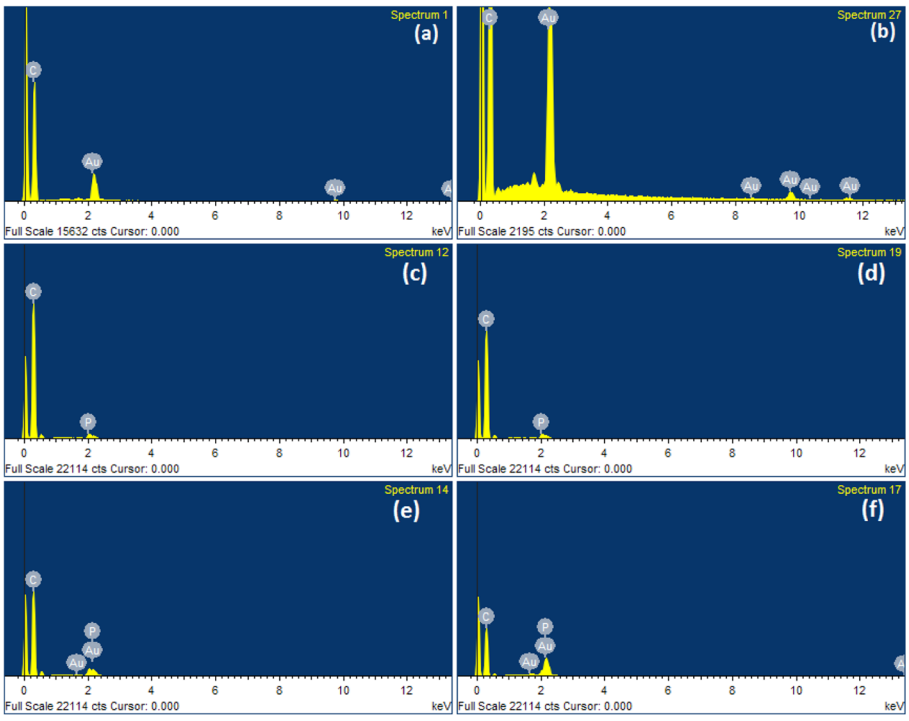


**Figure 8.** SEM-EDX spectra of CGN-25 (a), CGN-170 (b), CPN-25 (c), CPN-170 (d), CGPN-25 (e) and CGPN-170 (f).

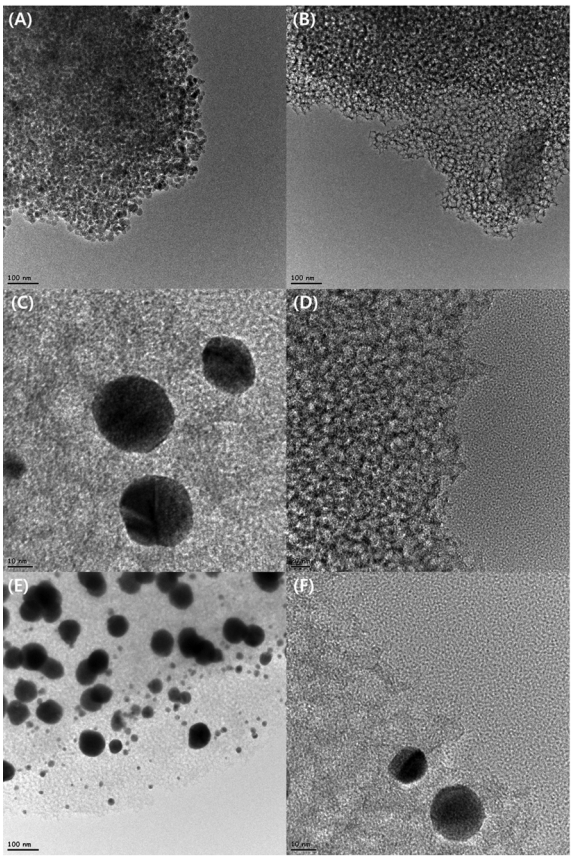


**Figure 9.** TEM images of NSB-25 (a), CC-25 (b), CGN-25 (c), CPN-25 (d) and CGPN-25 (e and f).

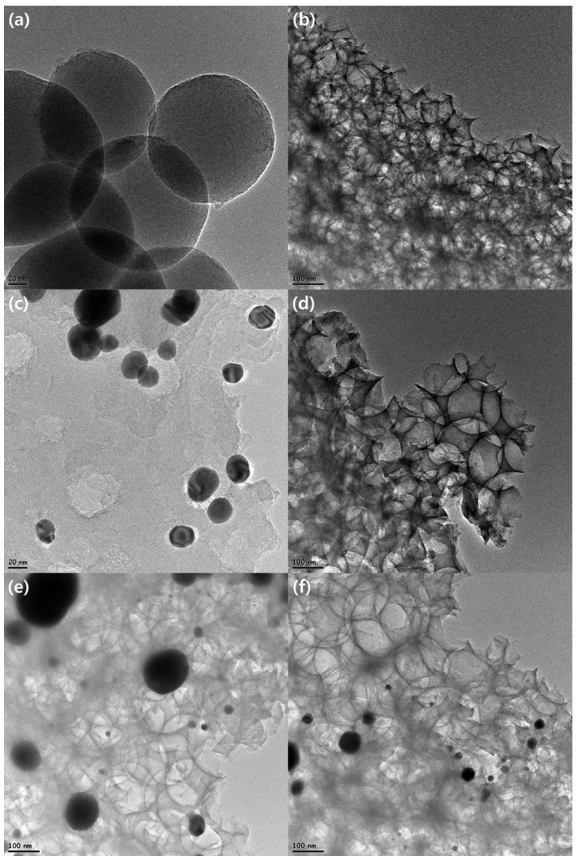


**Figure 10.** TEM images of NSB-170 (a), CC-170 (b), CGN-170 (c), CPN-170 (d) and CGPN-170 (e and f).

spectra recoded in the examined area of CGN-25/170, CPN-25/170 and CGPN-25/170 have shown strong signals for gold, phosphorus and combined (Au-P) along with carbon foundation, respectively (Figure 8).

**Characterization by TEM Analysis.** In addition, by comparing the high magnification TEM images of the NSB-25 template (Figure 9(A)) and replicated composite carbon materials (CC-25) (Figure 9(B)), it can be observed that the porous structure of the silica template is well imitated. The consistent hollow cores of hierarchically porous CC-25 were identical and strongly connected each other.[9] The TEM image of CGN-25 and CPN-25 confirms that the Au and P nanoparticles are homogeneously dispersed and adhere to the carbon cage cores (Figure 9(C) and 9(D)). While the TEM image of CGPN-25 shown combined Au and P nanoparticles on interconnected hierarchically hollow cores (~25 nm) of carbon structure (Figure 9(E) and 9(F)).

Subsequently, by comparing the high magnification TEM images of the NSB-170 template (Figure 10(a)) and replicated composite carbon materials (CC-170) (Figure 10(b)), it can be observed that the porous structure of the silica template is well imitated. The consistent hollow cores of hierarchically porous CC-170 were identical and strongly connected each other.[9] The TEM image of CGN-170 and CPN-170 confirms that the Au and P nanoparticles are homogeneously dispersed and adhere to the carbon cage cores (Figures 10(c) and 10(d)). While the TEM image of CGPN-170 shown combined Au and P nanoparticles on interconnected hierarchically wider hollow cores (~170 nm) of carbon structure (Figure 10(e)).

**Nitrogen Adsorption-desorption Study.** The total pore volume of the material was estimated from the amount of $N_2$ adsorption at relative pressure of about 0.995. The primary mesopore volume *Vp* was calculated from the slope of a linear portion of the *t*-plot in the pressure range above the pressure of nitrogen condensation in primary mesopores. Typical isotherms are shown in Figures 11 to 15, which represents a pore structure of type *IV* and confirms the well arranged mesopores. The BET surface area, BJH pore diameter, total pore volumes found are summarized in Table 1. The NSB-25 gave fair BET surface area (30 $m^2$/g), total pore volume (0.086 $cm^3$/g) and BJH pore diameter (116 Å). A large increase in BET surface area was observed (30-82 $m^2$/g) upon preparation of carbon cage (CC-25). Consequently, reduction in the BJH pore diameter from 116 to 58 Å and tiny rise in total pore volume from 0.086 to 0.120 $cm^3$/g was observed. On the another hand, small decrease in BET surface area 82 to 75 $m^2$/g in pore volume from 0.120 to 0.108 $cm^3$/g and in pore diameter from 58 to 57 Å was observed upon gold incorporation in carbon cage indicates that the internal pores of the CC-25 are occupied by the gold particles (CGN-25). Similarly, small decrease in BET

surface area (from 82 to 70 $m^2/g$), pore volume (from 0.120 to 0.105 $cm^3/g$) and slightly increased pore diameter (from 58 to 60 Å) were noticed upon phosphorus insertion in carbon matrix. It indicates that the pores of carbon matrix (CC-25) are filled by the phosphorus elements in CPN-25. Moreover, the decrease in BET surface area (from 75 to 40 $m^2/g$), pore volume (from 0.108 to 0.075 $cm^3/g$) and small increment in pore diameter (from 57 to 76 Å) were found by phosphorus incorporation in CGN-25. It is again supports the phenomenon of filling the internal pores of CGN-25 by the phosphorus elements in CGPN-25.

The NSB-170 gave fair BET surface area (163 $m^2/g$), total pore volume (0.290 $cm^3/g$) and BJH pore diameter (71 Å). A large increase in BET surface area was observed (163-212 $m^2/g$) upon preparation of CC-170. Consequently, addition in the BJH pore diameter from 71 to 162 Å and rise

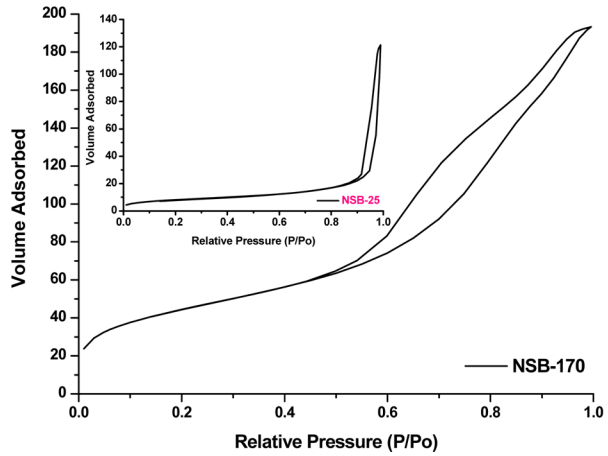


**Figure 11.** Nitrogen adsorption-desorption isotherms of NSB-25 and NSB-170.

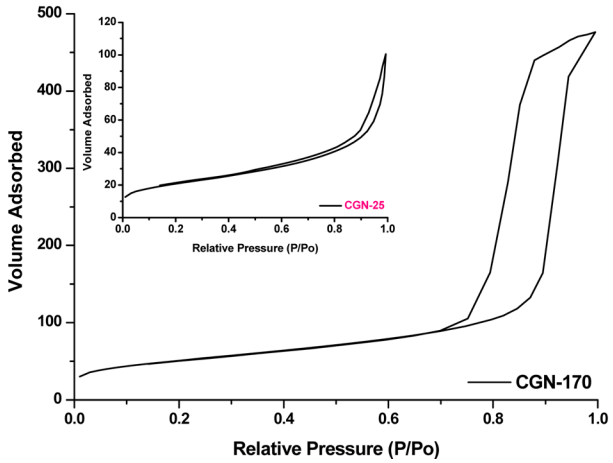


**Figure 13.** Nitrogen adsorption-desorption isotherms of CGN-25 and CGN-170.

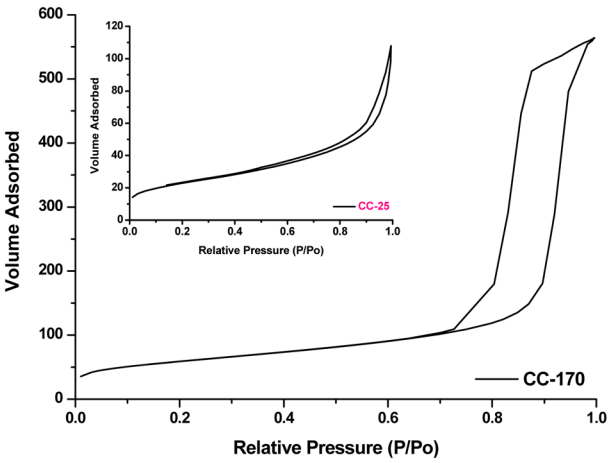


**Figure 12.** Nitrogen adsorption-desorption isotherms of CC-25 and CC-170.

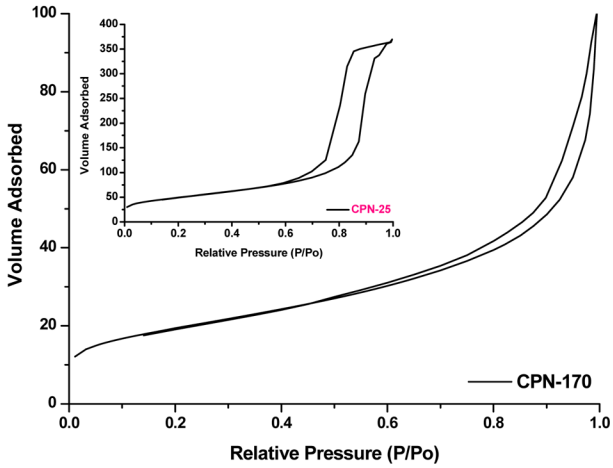


**Figure 14.** Nitrogen adsorption-desorption isotherms of CPN-25 and CPN-170.

**Table 1.** Physico-chemical data of NSB, CC, CGN, CPN and CGPN (25 and 170 nm)

| Sr. No. | Compound | BET Surface Area ($m^2/g$) | Total Pore Volume ($cm^3/g$) | BJH Pore Diameter (Å) | Langmuir Surface Area ($m^2/g$) |
|---|---|---|---|---|---|
| 1 | NSB-25 | 30 | 0.086 | 116 | 38 |
| 2 | CC-25 | 82 | 0.120 | 58 | 105 |
| 3 | CGN-25 | 75 | 0.108 | 57 | 96 |
| 4 | CPN-25 | 70 | 0.105 | 60 | 94 |
| 5 | CGPN-25 | 40 | 0.075 | 76 | 53 |
| 6 | NSB-170 | 163 | 0.290 | 71 | 219 |
| 7 | CC-170 | 212 | 0.857 | 162 | 271 |
| 8 | CGN-170 | 184 | 0.737 | 160 | 246 |
| 9 | CPN-170 | 178 | 0.558 | 125 | 238 |
| 10 | CGPN-170 | 172 | 0.628 | 146 | 220 |

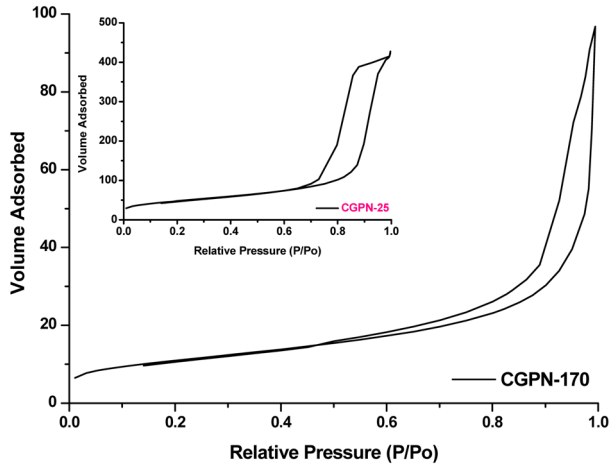


**Figure 15.** Nitrogen adsorption-desorption isotherms of CGPN-25 and CGPN-170.

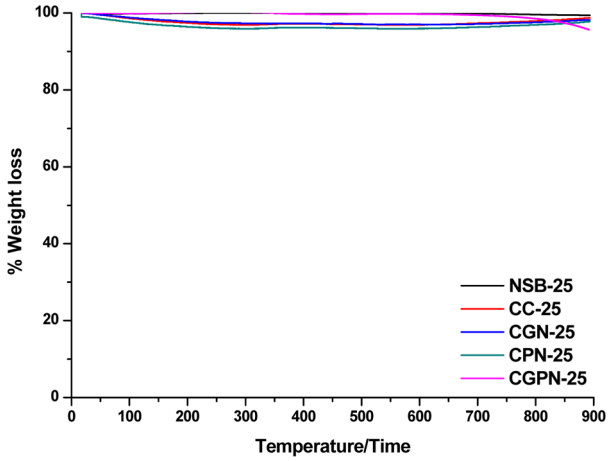


**Figure 16.** Thermo-gravimetric analysis **(**TGA) curves of NSB-25, CC-25, CGN-25, CPN-25 and CGPN-25.

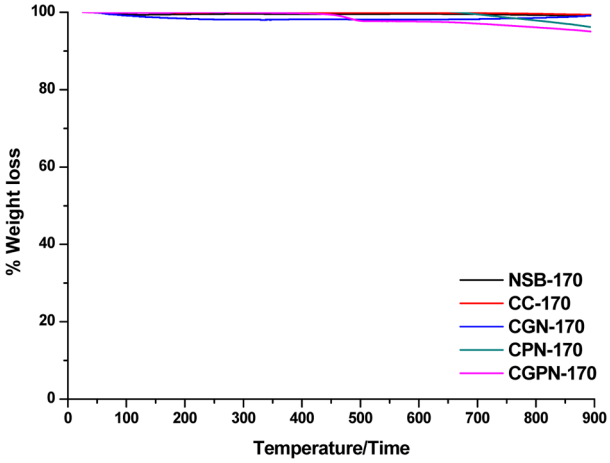


**Figure 17.** Thermo-gravimetric analysis **(**TGA) curves of NSB-170, CC-170, CGN-170, CPN-170 and CGPN-170.

in total pore volume from 0.290 to 0.857 $cm^3/g$ was observed. On the another hand, small decrease in BET surface area 212 to 184 $m^2/g$ in pore volume from 0.857 to 0.737 $cm^3/g$ and in pore diameter from 162 to 160 Å was observed upon gold incorporation in CC-170 indicates that the internal pores of the CC-170 are occupied by the gold particles (CGN-170). Similarly, small decrease in BET surface area 212 to 178 $m^2/g$ in pore volume from 0.857 to 0.558 $cm^3/g$ and in pore diameter from 162 to 125 Å was observed upon phosphorus addition in carbon cage indicates that the internal pores of the CC-170 are occupied by the phosphorus particles (CPN-170). Moreover, tiny decrease in BET surface area 184 to 172 $m^2/g$ in pore volume from 0.737 to 0.628 $cm^3/g$ and small decrease in pore diameter from 160 to 146 Å was observed upon phosphorus incorporation in CGN-170 indicates that the internal pores of the CGN-170 are occupied by the phosphorus particles (CGPN-170). The experiment result indicates that the structure of all nanocomposites are maintained after modification.

**Thermal Analysis (TGA/ICP/Elemental Analysis).** Thermo-gravimetric curves (Figures 16 and 17) shown minor weight losses of about < 10% occurred from 25 to 900 $^oC$ for NSB, CC, CGN, CPN and CGPN (25/170 nm). This weight loss can be mainly attributed due to the removal of water molecules and further carbonization between 100 to 900 $^oC$. Elemental analysis data of CC-25 indicate that carbonization (> 900 $^oC$) is almost completely achieved, with < 6% oxygen and hydrogen remaining, respectively, thus suggesting that a pure carbon, homologous framework is obtained. ICP analysis of CGN-25 and CPN-25 showed 11.0 wt % and 0.9 wt % gold and phosphorus respectively. ICP measurement of CGPN-25 revealed 10.9 wt % and 0.9 wt % combined gold and phosphorus which is required to be present to make carbon gold phosphorus nanocomposite (CGPN-25).

Elemental analysis data of CC-170 indicate that carbonization (> 900 $^oC$) is almost completely achieved, with < 5% oxygen and hydrogen remaining, respectively, thus suggesting that a pure carbon, homologous framework is obtained. ICP analysis of CGN-170 and CPN-170 showed 10.2 wt % and 1.5 wt % gold and phosphorus respectively. ICP measurement of CGPN-170 revealed 4.8 wt % and 3.3 wt % combined gold and phosphorus which is required to be present to make carbon gold phosphorus nanocomposite (CGPN-170).

## References

1. Mayani, S. V.; Mayani, V. J.; Park, S. K.; Kim, S. W. *Mater. Lett.* 2012, **82**, 120.
2. Mayani, V. J.; Mayani, S. V.; Lee, Y.; Park, S. K. *Sep. Purif. Technol*. **2011**, 80, 90.
3. Mayani, V. J.; Mayani, S. V.; Kim, S. W. *Mater. Lett.* **2012**, 87, 90.
4. Perrin, D. D.; Armarego, W. L. F.; Perrin, D. R. *Purification of Laboratory Chemicals*; Pergamon, New York: 1981.
5. 5. Guo, X.; Liu, X.; Xu, B.; Dou, T. *Colloids Surf., A* **2009**, 345, 141.
6. Kao, L. H.; Hsu, T. C. *Mater. Lett*. **2008**, 62, 695.
7. Vermisoglou, E. C.; Romanos, G. E.; Tzitzios, V.; Karanikolos, G. N.; Akylas, V.; Delimitis, A.; Pilatos, G.; Kanellopoulos, N. K. *Microporous Mesoporous Mater.* **2009**, 120, 122.
8. Yang, G. W.; Gao, G. Y.; Wang, C.; Xu, C.-L.; Li, H. -L. *Carbon* **2008**, 46, 747.
9. Li, Q.; Jiang, R.; Dou, Y.; Wu, Z.; Huang, T.; Feng, D.; Yang, J.; Yu, A.; Zhao, D. *Carbon* **2011**, *49*, 1248.